Journal of Applied Fluid Mechanics, Vol. 16, No. 1, pp. 1-7, 2023.
Available online at www.jafmonline.net, ISSN 1735-3572, EISSN 1735-3645.
https://doi.org/10.47176/jafm.16.01.1366

Instabilities of Transonic Turbulent Flow over a Flat-Sided Wedge

A. Kuzmin†

Department of Fluid Dynamics, St. Petersburg State University, 28 University Ave., St. Petersburg 198504, Russia

†*Corresponding Author Email: a.kuzmin@spbu.ru*

(Received June 9, 2022; accepted August 8, 2022)

ABSTRACT

The transonic turbulent two-dimensional airflow over a symmetric flat-sided double wedge is studied numerically. Solutions of the Reynolds-averaged Navier-Stokes equations are obtained with ANSYS-18.2 CFX finite-volume solver of second order accuracy on a fine mesh. The solutions demonstrate an extreme sensitivity of the flow field and lift coefficient to variation of the angle of attack α or free-stream Mach number M_∞. Non-unique flow regimes and hysteresis in certain bands of α and M_∞ are identified. Interaction of shock waves and local supersonic regions is discussed. The study confirms a concept of shock wave instability due to a coalescence/rupture of supersonic regions. In addition to the instability of shock wave locations, the numerical simulation shows a buffet onset, i.e., self-exciting oscillations due to instability of a boundary layer separation at the rear of wedge. Curious flow regimes with positive lift at negative angles α and, vice versa, with negative lift at positive angles α, are pointed out. A piecewise continuous dependence of the lift coefficient on two free-stream parameters, α and M_∞, is discussed.

Keywords: Local supersonic regions; Shock waves; Interaction; Boundary-layer separation; Oscillations.

NOMENCLATURE

C_L	lift coefficient	t	time
c_p	specific heat at constant pressure	T	static temperature
L	lift force	URANS	Unsteady Reynolds-Averaged Navier-Stokes
LSR	Local Supersonic Region		
M	Mach number	x, y	non-dimensional Cartesian coordinates
M_∞	free-stream Mach number	α	angle of attack
U	x-component of flow velocity	γ	ratio of specific heats
V	y-component of flow velocity	Γ_1	inflow part of boundary
p	static pressure	Γ_2	outflow part of boundary
SW	Shock Wave	ρ	density

1. INTRODUCTION

There exist airfoils that admit extremely high sensitivity of transonic flow to free-stream parameters. Numerical studies of laminar flow over an X63T18S airfoil demonstrated essential changes of the flow field under small deviations of the free stream from on-design conditions (Pfenninger *et al.* 1986). Later, numerical simulations of inviscid flow over four special airfoils showed the lift coefficient hysteresis in narrow bands of the angle of attack (Jameson 1991). Then non-unique flow regimes and high sensitivity to free-stream Mach number were revealed for symmetric airfoils at the vanishing angle of attack (McGrattan 1992; Hafez and Guo 1999a, 1999b).

Kuzmin (2005) suggested that the hysteresis and non-uniqueness occur if an airfoil involves a straight segment or nearly flat arc. Such a segment/arc provokes the arising of two local supersonic regions on the same side of airfoil. A coalescence/rupture of the regions (under variation of free-stream parameters) proceeds abruptly and produces essential changes in shock wave locations and entire structure of the flow. This concept was confirmed numerically for both turbulent and inviscid flows over symmetric and asymmetric airfoils and wings (Kuzmin 2012, 2014; Ryabinin 2015).

We notice that airfoils involving nearly flat parts have become of considerable practical interest in recent years because they arise as solutions of up-to-date aerodynamic optimization problems (Destarac *et al.* 2018; Chen and Fidkowski 2019).

A most simple explanation of the instability of shock wave locations was suggested for transonic flow over a flat-sided double wedge (Kuzmin 2020). The explanation is based on an analysis of types of shock wave reflection from the wedge near its corner points under variation of free-stream conditions. In particular, a transition from the regular to Mach reflection is shown to trigger a rupture of the supersonic region and a jump of the shock location upstream. In addition to the instability of shock wave locations, the turbulent flow exhibits a conventional buffet onset at the rear of wedge.

In this paper, we consider turbulent transonic flow over the aforementioned double wedge and focus on the flow structure and hysteresis under variation of the angle of attack. In Sections 2 and 3 we formulate the boundary-value problem and describe a numerical method. Then in Section 4 we analyze locations of supersonic regions and their effect on the lift coefficient at three free-stream Mach numbers M_∞. Section 5 addresses multiple regimes at the vanishing angle of attack α in a band of M_∞. Finally, in Section 6 we discuss a surface illustrating the lift coefficient as a function of α and M_∞, which is similar to the surface discussed in (Kuzmin 2005) for a smooth airfoil and inviscid flow.

2. FORMULATION OF THE PROBLEM

The double wedge under consideration is given by the expressions:

$$\left.\begin{array}{ll} \text{(a) nose:} & y(x)= \pm 0.4x/3 \quad \text{at} \quad 0\le x<0.3, \\ \text{(b) flat midpart:} & y(x)= \pm 0.04 \quad \text{at} \quad 0.3\le x\le 0.7, \\ \text{(c) tail:} & y(x)=\pm 0.4(1-x)/3 \quad \text{at} \quad 0.7< x\le 1.0, \end{array}\right\} \quad (1)$$

where Cartesian coordinates (x,y) are normalized by the wedge length l_1=0.5 m. For numerical simulation of 2D airflow over wedge (1), we use the unsteady Reynolds-averaged Navier-Stokes (URANS) equations (Tennekes and Lumley 1992) with respect to flow temperature $T(x,y,t)$, density $\rho(x,y,t)$, and velocity components $U(x,y,t)$, $V(x,y,t)$, where t is time. The air is assumed to be a perfect gas. The flow pressure $p(x,y,t)$ is related to density and temperature by the equation of state $p=\rho RT$, where $R=c_p-c_p/\gamma$ is specific gas constant, γ=1.4 is the ratio of specific heats, and c_p=1004.4 J/(kg K) is specific heat at constant pressure.

The computational domain is bounded by wedge (1) and a pair of circular arcs Γ_1 and Γ_2 of radius 145 with endpoints x=0, y=±100, see Fig. 1. On Γ_1, we set the angle of attack α, Mach number M_∞<1, and temperature T_∞=250 K, which determine velocity components $U_\infty=M_\infty a_\infty \cos\alpha$ and $V_\infty=M_\infty a_\infty \sin\alpha$, where $a_\infty=(\gamma RT_\infty)^{1/2}$. The level of free-stream turbulence is set to 1%.

On Γ_2, we prescribe the static pressure $p_\infty=3\times10^5$ N/m^2. The no-slip condition and vanishing heat flux are imposed on the wedge. The Reynolds number calculated using the wedge length l_1 is 3.0×10^7.

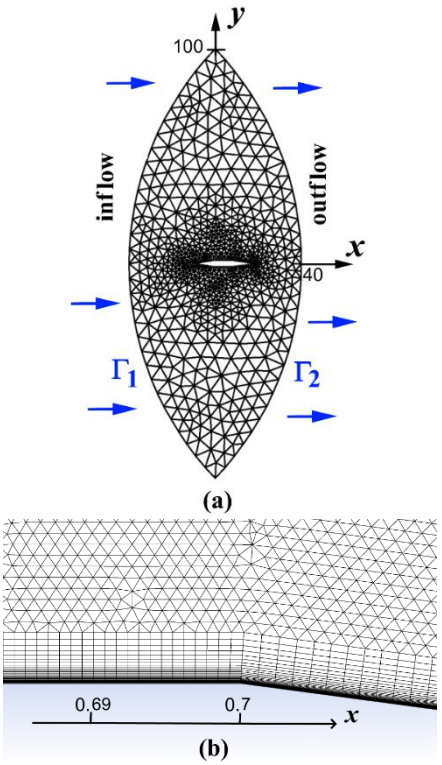

Fig. 1. (a) Schematic of the computational domain and mesh, (b) a fragment of the mesh near the upper rear corner of wedge; the boundary layer thickness is about 0.006.

3. NUMERICAL METHOD

The system of URANS equations was solved with ANSYS-18.2 CFX finite-volume solver (see ANSYS 2022). We used the k-ω SST turbulence model which is known to reasonably predict transonic flows with boundary layer separation (Menter 2009). 2D meshes in the plane (x,y) were constituted by quadrangular cells in 40 mesh layers on wedge (1) and by triangular cells in the remaining region. Principal computations were performed on a mesh of 988,238 cells. Mesh nodes were clustered near the wedge for an accurate resolution of shocks and boundary layer. The non-dimensional distance $y+$ from the wedge to the first mesh node was less than 1.2. The 3D mesh used by ANSYS CFX was obtained by an extrusion of the 2D mesh in the z-direction from z=0 to $z=l_2$=0.002 m. Test computations on a uniformly refined mesh of about 1.5×10^6 elements demonstrated only an insignificant discrepancy between solutions calculated on the basic and fine meshes, see below Table 1.

For the global time-stepping, we used an implicit backward Euler scheme. The timestep of 10^{-5} s produced solutions indistinguishable from those obtained at the time step of 5×10^{-6} s. The root-mean-square Courant-Friedrichs-Lewy number was smaller than 2.

Table 1. Results of test computations of C_L on three different meshes.

M_∞, α	Mesh	$C_{L,max}$	$C_{L,min}$
M_∞=0.839 α=0°	coarse 617,182 cells	0.053	0.033
	basic 988,238 cells	0.048	0.028
	fine 1,482,056 cells	0.046	0.026
M_∞=0.839 α=0.4°	coarse	0.133	0.036
	basic	0.128	0.031
	fine	0.126	0.030
M_∞=0.840 α=0°	coarse	0.056	0.024
	basic	0.050	0.019
	fine	0.048	0.018
M_∞=0.840 α=0.4°	coarse	0.145	0.035
	basic	0.140	0.029
	fine	0.138	0.027

3. FLOW HYSTERESIS AT GIVEN M_∞ UNDER VARIATION OF THE ANGLE OF ATTACK

First, we considered the case α=0.5°, M_∞=0.839 and used the free-stream parameters as initial data. The obtained solution revealed a large local supersonic region (LSR) above the wedge and two smaller LSRs below it, see Fig. 2. The upper LSR is terminated by a shock wave (SW), which oscillates between a normal approach to the flat part of wedge and a regular reflection from the rear ramp. The aerodynamic force $\vec{F}$ is obtained by integration of the pressure p over the wedge surface. Due to the shock-induced boundary-layer separation, the force $\vec{F}$ exhibits intricate oscillations in time, and so does the lift L which is a component of $\vec{F}$ in the normal direction to the free stream. The obtained lift coefficient $C_L=2L/(\rho_\infty\ a_\infty^2\ M_\infty^2\ l_1\ l_2)$ oscillates between $C_{L,min}$=0.05 and $C_{L,max}$=0.16, see Fig. 3. The frequency of oscillations is 62 Hz.

Then we performed flow simulations at smaller angles of attack step-by-step from α=0.5° to α=−0.04°. At each step, flow parameters obtained at the previous value of α were used as initial data. The simulations showed that the amplitude of oscillations decreases with decreasing α, see domain 1 in Fig. 4, and eventually it vanishes at point A (α=−0.04°). Though the upper LSR shrinks on the wedge and SW shifts upstream to the corner point x=0.7, y=0.04, the general flow pattern persists, and lift coefficient remains positive.

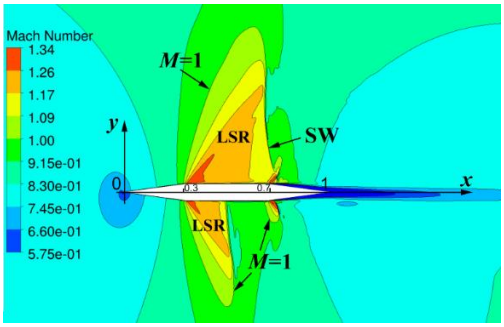

Fig. 2. Instant Mach number contours $M(x,y,t)=(U^2+V^2)^{1/2}/a$=const in a vicinity of wedge (1) at M_∞=0.839, α=0.5°.

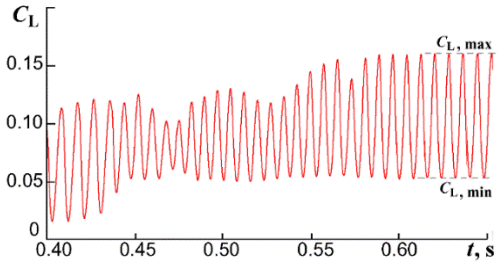

Fig. 3. Development of lift coefficient oscillations at M_∞=0.839, α=0.5°.

If the angle α drops below −0.04°, then SW moves further upstream and meets the horizontal portion of wedge. That is why the incident angle changes abruptly, and regular reflection of the shock cannot exist. This implies formation of a Mach reflection with subsonic velocities downstream of the Mach stem. Therefore, the upper LSR ruptures, and SW shifts upstream at a distance from the corner x=0.7, y=0.04. This is accompanied by a coalescence of LSRs below the wedge. The lift coefficient becomes oscillatory again and negative, as pointed out by the left arrow in Fig. 4.

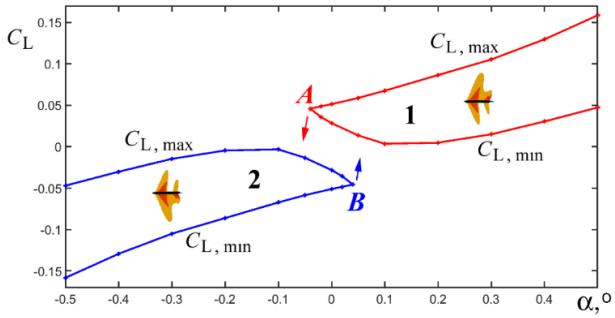

Fig. 4. Margins of lift coefficient oscillations versus the angle of attack in the flow over wedge (1) at M_∞=0.839. Sketches next to the curves hint at locations of supersonic regions.

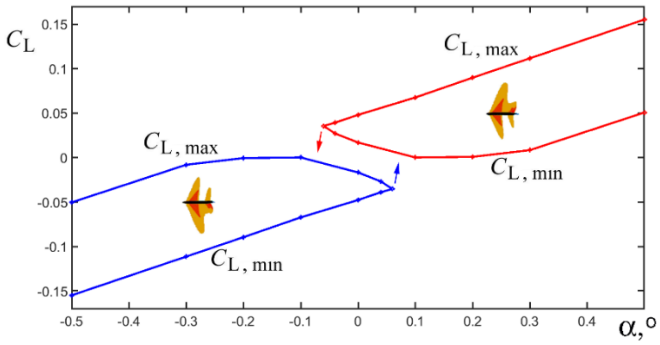

Fig. 5. Margins of lift coefficient oscillations versus the angle of attack in the flow over wedge (1) at M_∞=0.840.

Further computations at larger and smaller values of α step-by-step in the band $-0.5° \le \alpha \le 0.04°$ yield the full boundary of domain 2. In this flow regime, there is a single LSR below the wedge and two LSRs above it. Meanwhile, when α exceeds 0.04° (see point B in Fig. 4), computations show an inverse transition from domain 2 to domain 1. Therefore, in the band $-0.04° \le \alpha \le 0.04°$, there is a hysteresis in the dependence of C_L on α.

At the larger free-stream Mach number M_∞=0.840, numerical simulations yield a similar plot of C_L versus α, in which the hysteresis expands to the band $-0.06° \le \alpha \le 0.06°$, see Fig. 5. In particular, the flow obtained at α=0° in the regime with $C_L>0$ is depicted in Fig. 6. The flow pattern in the regime with $C_L<0$, α=0° can be obtained by reflection of Fig. 6 about the *x*-axis.

We mention that an employment of a smaller computational domain would introduce a noticeable error in the numerical solutions. For example, a downstream shift of the inflow boundary Γ_1 to a position in which it intersects the *x*-axis at the point *x*=−25 instead of *x*=−40 would mean the imposing of M_∞=0.840 at this point. Meanwhile, the solution depicted in Fig. 6b shows that the actual value is *M*=0.8395.

Table 1 illustrates results of test computations of C_L on three different meshes. As seen, the discrepancies between values obtained on the basic and fine meshes are small enough and do not affect locations of curves in Figs. 4 and 5.

Figure 7 demonstrates Mach number contours over wedge (1) obtained with an ANSYS Fluent solver (instead of ANSYS CFX) on the same computational mesh. A comparison of the flow fields displayed in Figs. 6a and 7 shows their good agreement.

At M_∞=0.837, α=0.5° computations produce a flow with one LSR above the wedge and two LSRs below it, as in the previous cases with larger Mach numbers. However, a decrease of α to values smaller than 0.02° yields a transition to a steady flow with four LSRs, see the upper arrow in Fig. 8. Then further decrease of α to values smaller than −0.05° results in a flow with two LSRs above the wedge and one LSR below it.

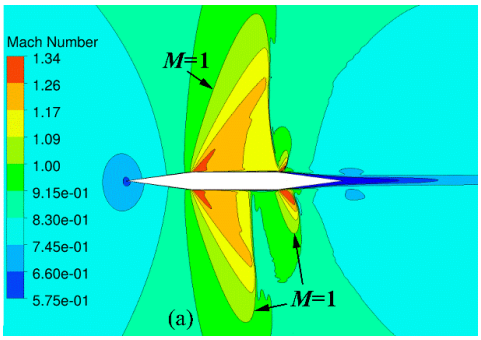

(a) a vicinity of the wedge

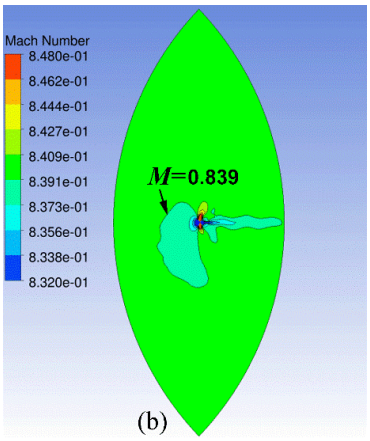

(b) the far field

Fig. 6. Instant Mach number contours in the flow regime with $C_L>0$ at M_∞=0.840, α=0°.

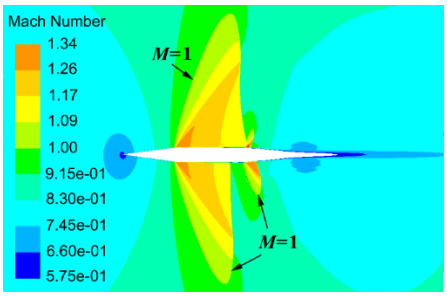

Fig. 7. Mach number contours in the flow regime with $C_L>0$ at M_∞=0.840, α=0° obtained with an ANSYS Fluent solver.

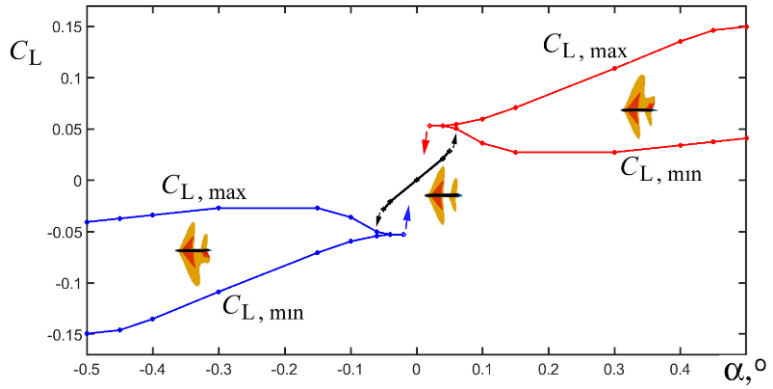

Fig. 8. Lift coefficient versus the angle of attack in the flow over wedge (1) at M_∞=0.837.

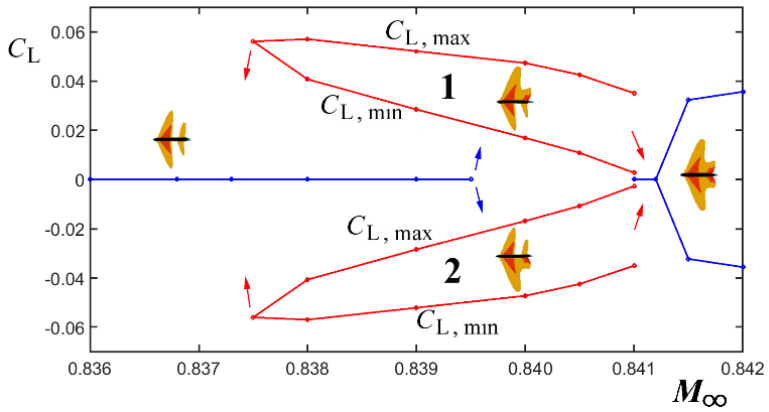

Fig. 9. Margins of lift coefficient oscillations versus the free-stream Mach number M_∞ at α=0°.

4. FLOW NON-UNIQUENESS AT THE VANISHING ANGLE OF ATTACK

The asymmetric solutions with three LSRs obtained in Section 4 at zero angle of attack and M_∞=0.840 or M_∞=0.839 can be employed as initial values for flow simulation at larger and smaller M_∞. The simulation showed that the asymmetric flows persist at $0.8375 \le M_\infty \le 0.841$, see domains 1 and 2 in Fig. 9. For instance, domain 1 corresponds to the same flow pattern with a regular reflection of SW from the rear ramp as in Figs. 6,7. The amplitude of lift coefficient oscillations decreases when M_∞ decreases, and eventually it vanishes at M_∞=0.8375.

If M_∞ becomes smaller than 0.8375, then the asymmetric flows cannot exist at α=0°, as SW (being shifted upstream) meets the horizontal part of wedge. This entails formation of a Mach reflection of SW and transition to a steady symmetric flow with a pair of LSRs both below and above the wedge. Further variation of M_∞ shows that the symmetric flow with C_L=0 is stable in the band $0.835 \le M_\infty \le 0.8395$. At larger Mach numbers $0.8395 < M_\infty < 0.841$, the symmetric flow is unstable, that is why any perturbation triggers a transition to the asymmetric flow with C_L>0 or C_L<0, see Fig. 9.

The upper bound for the asymmetric flows with three LSRs, which correspond to domains 1 and 2 in Fig. 9, is M_∞=0.841. At larger Mach numbers, there is a transition to the symmetric flow with a single LSR both below and above the wedge. At M_∞>0.8412, the symmetric flow exhibits oscillations due to the instability of boundary-layer separation at the rear of wedge.

A comparison of Fig. 9 with results obtained for p_∞=150,000 N/m^2 in (Kuzmin 2020, Fig. 5) shows that the amplitude of lift coefficient oscillations rises with increasing p_∞ and, consequently, increasing Reynolds number.

5. DEPENDENCE OF LIFT COEFFICIENT ON BOTH PARAMETERS, ANGLE OF ATTACK AND M_∞.

The piecewise continuous surface displayed in Fig. 10 illustrates a dependence of C_L on M_∞ and α in the flow regimes with C_L>0. The lower part of the surface shows the lift coefficient in the steady flow with four LSRs on wedge (1). The upper parts $C_{L,max}$ and $C_{L,min}$ determine margins of lift coefficient oscillations in the flow with three LSRs. Typically, the amplitude of oscillations increases with increasing angle α. Meanwhile, there are drops of the amplitude and $C_{L,max}$ near the free-stream parameters α=0.5°, M_∞=0.835. This is explained by a shift of SW foot to a position at the very corner x=0.7, y=0.04 which means a disappearance of the local supersonic region over the corner. As a consequence, the subsonic flow expansion over the convex wall is accompanied by an increase in the static pressure (see Fig. 11) and by a drop in C_L. In

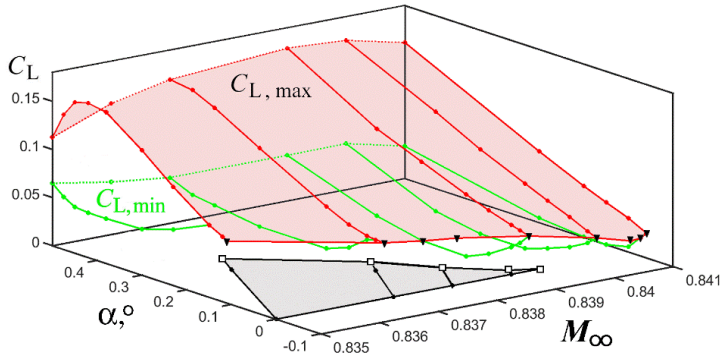

Fig. 10. Lift coefficient C_L as a function of α and M_∞ in flow regimes with $C_L>0$ and three or four LSRs on wedge (1) at $0.835 \le M_\infty \le 0.841$.

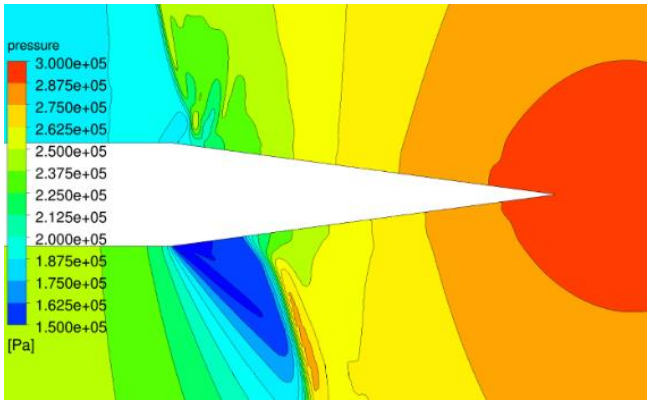

Fig. 11. Instant pressure distributions over rear ramps at M_∞=0.835, α=0.5°.

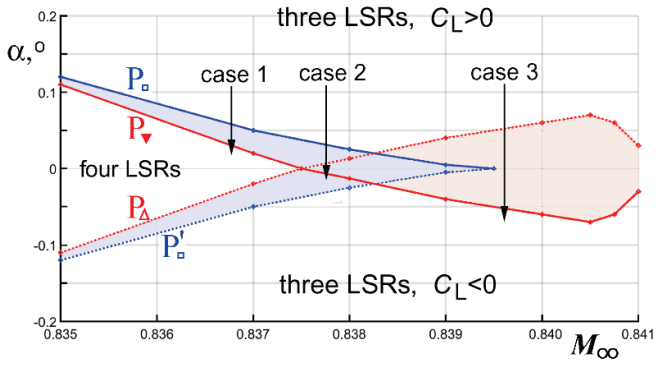

Fig. 12. Curves in the plane (α, M_∞) that show boundaries of different flow regimes over wedge (1).

addition, a development of the larger LSR over the lower ramp decreases the static pressure beneath the wedge and contributes to the lift coefficient drop.

A projection $P_□$ of the 3D curve marked by squares in Fig. 10 onto the plane (α, M_∞) determines maximum angles of attack for the flow regime with four LSRs, see Fig. 12. If α becomes larger than these values, then LSRs get into coalescence on the upper surface of wedge and yield a transition to flow regime with three LSRs.

A projection $P_▼$ of the 3D curve marked by triangles in Fig. 10 onto the plane (α, M_∞) determines minimum angles of attack for the regime with three LSRs. If α becomes smaller than these values, and M_∞<0.8375 (case 1 in Fig. 12), then the LSR ruptures on the upper surface of wedge and triggers a transition to flow regime with four LSRs.

In order to trace all types of transitions, we need to take into consideration boundaries $P'_□$ and $P_Δ$ of flow regimes with C_L<0, see the dashed curves in Fig. 12. The surface C_L(α, M_∞) illustrating the regimes with C_L<0 can be obtained by a 180 degree rotation of the surface displayed in Fig. 10 about the M_∞-axis. Projections $P'_□$ and $P_Δ$ of its edges onto the plane (α, M_∞) are symmetric to $P_□$ and $P_▼$ about the line α=0°. We notice that the full surface C_L(α, M_∞) looks

like the one obtained for inviscid flow over a smooth airfoil in (Kuzmin 2005, Fig. 8).

At $0.8375<M_\infty<0.838$, if α decreases, e.g., from 0.2° to values a bit smaller than those determined by curve P▼, then the LSR ruptures on the upper surface of wedge and yields the flow with four LSRs and $C_L<0$ (case 2 in Fig. 12). Further decrease of α leads to flow regime with $C_L<0$ and three LSRs.

At $M_\infty>0.83825$, if α decreases from 0.2° to smaller values than those determined by curve P▼, then the LSR ruptures on the upper surface of wedge and yields the flow with $C_L<0$ and three LSRs (case 3 in Fig. 12).

Similar three cases are true at increasing α from −0.2° to 0.2°. Shaded areas in Fig. 12 point out domains in which there is hysteresis accompanying transitions between different regimes of the flow.

5. CONCLUSION

The transonic flow simulations over wedge (1) at the Reynolds number of 3.0×10^7 revealed an extreme sensitivity of the lift coefficient and flow structure to variation of free-stream parameters. There exist flow hysteresis and non-uniqueness in certain bands of the angle of attack α and Mach number M_∞. A theoretical interpretation of the hysteresis and non-uniqueness is based on the instability of shock wave reflection from the wedge in vicinities of its rear corners. Flow regimes with three local supersonic regions typically exhibit oscillations caused by the separation of boundary layer at the rear. Margins of the oscillations shrink with decreasing angle α.

ACKNOWLEDGEMENTS

This research was performed using computational resources provided by the Computational Center of St. Petersburg State University (http://cc.spbu.ru). The work was supported by a grant from the University (ID 93935136).

REFERENCES

ANSYS Fluids (2022) Computational Fluid Dynamics. https://www.ansys.com/products/fluids

Chen, G. and K. Fidkowski (2019). Output-based mesh adaptation for variable-fidelity multipoint aerodynamic optimization. *AIAA Paper* 2019-3057, 1–19.

Destarac, D., G. Carrier, G. R. Anderson, S. Nadarajah, D. J. Poole, J. C. Vassberg, D. W. Zingg (2018). Example of a pitfall in aerodynamic shape optimization. *AIAA Journal* 56, 1532–1540.

Jameson, A. (1991). Airfoils admitting non-unique solutions of the Euler equations. *AIAA Paper* 91-1625, 1–13.

Hafez, M. M. and W. H. Guo, (1999a). Nonuniqueness of transonic flows. *Acta Mechanica* 138, 177–184.

Hafez, M. M. and W. H. Guo (1999b). Some anomalies of numerical simulation of shock waves. Pt. 1. Inviscid flows. *Computers and Fluids* 28, 701–719.

Kuzmin, A. (2005). Instability and bifurcation of transonic flow over airfoils. *AIAA Paper* 2005-4800, 1–8.

Kuzmin, A. (2012). Non-unique transonic flows over airfoils. *Computers and Fluids* 63, 1–8.

Kuzmin, A. (2014). On the lambda-shock formation on ONERA M6 wing. *International Journal of Applied Engineering Research* 9, 7029–7038.

Kuzmin, A. (2020). Transonic flow bifurcations over a double wedge. *Journal of Physics: Conference Series* 1697, Article ID 012207, 1–6.

McGrattan, K. (1992). Comparison of transonic flow models. *AIAA Journal* 30, 2340–2343.

Menter, F. R. (2009). Review of the shear-stress transport turbulence model experience from an industrial perspective. *International Journal of Computational Fluid Dynamics* 23, 305–316.

Pfenninger, W., J. K. Viken, C. S. Vemuru, G. Volpe, (1986). All laminar supercritical LFC airfoils with laminar flow in the main wing structure. *AIAA* Paper 86-2625, 1–45.

Ryabinin, A. (2015). Transonic flow past symmetrical unswept and swept wings with elliptic nose. *ARPN Journal of Engineering and Applied Sciences* 10, 9359-9363.

Tennekes, H. and J. L. Lumley (1992). A first course in turbulence (14. print. ed.). MIT Press, Cambridge, Massachusetts, USA.